High-frame-rate Volumetric Porcine Cardiac Imaging

Wei, Luxi; Wahyulaksana, Geraldi ; Boni, Enrico; Noothout, Emile; Tortoli, Piero; van der Steen, A.F.W.; de Jong, Nico; Verweij, Martin; Vos, Hendrik J.; More Authors

DOI
10.1109/IUS51837.2023.10307927

Publication date
2023

Document Version
Final published version

Published in
IUS 2023 - IEEE International Ultrasonics Symposium, Proceedings

High-frame-rate Volumetric Porcine Cardiac Imaging

Luxi Wei, Geraldi Wahyulaksana, Maaike te Lintel Hekkert, Daniel Bowen, Robert Beurskens, Enrico Boni, Alessandro Ramalli, Emile Noothout, Dirk J. Duncker, Piero Tortoli, Antonius van der Steen, Nico de Jong, Martin Verweij, and Hendrik J. Vos

2023 IEEE International Ultrasonics Symposium (IUS) | 979-8-3503-4645-9/23/$31.00 ©2023 IEEE | DOI: 10.1109/IUS51837.2023.10307927

***Abstract*—Volumetric echocardiography can potentially give a more complete picture of cardiac dynamics than its two-dimensional (2D) counterpart. Current clinical volumetric imaging probes have relatively low frame rates, and often require ECG gating to stitch together an entire volume. This makes measuring fast dynamics of the heart as well as imaging patients with irregular heartbeats difficult. We have previously designed and manufactured 2D sparse arrays with elements seeded in a density-tapered spiral pattern for cardiac imaging. Using these prototypes, we demonstrate in this paper the first high-frame-rate volumetric closed-chest porcine cardiac as well as open-chest myocardial blood flow results. These preliminary results suggest the potential of performing high-frame-rate volumetric cardiac imaging using the sparse spiral arrays.**

***Index Terms*—3D, volumetric, echocardiography, high-frame-rate, contrast-enhanced, 2D sparse arrays, 2D spiral arrays**

I. Introduction

Two-dimensional (2D) echocardiography is a routine diagnostic tool in the clinics for a variety of cardiovascular disorders: the left ventricular volume is used to diagnose cardiomyopathy [1]; Doppler ultrasound can be used to image blood flow around the heart valves and between chambers to look for valve defects and congenital heart defects [2]; and contrast-enhanced ultrasound can be used to look for myocardial infarcts and blood flow characteristics [3]. However, since the heart is a 3-dimensional (3D), highly dynamic structure, parameters that are measured in 2D may be severely operator-dependent and reliant on geometrical assumptions [4].

In this paper, we present the results from contrast-enhanced high-frame-rate volumetric porcine cardiac imaging experiments. Using our previously described sparse arrays with elements seeded in a density-tapered spiral pattern [5], [6], both closed- and open-chest experiments were performed for different purposes. By imaging microbubbles inside the cardiac chambers in closed-chest experiments, we could visualize the shape of the right and left ventricles throughout most of the cardiac cycle without ECG stitching. We could also estimate the single-heartbeat end-diastolic left ventricular volume in 3D. Through open-chest experiments, we visualized 3D coronary vasculature tree feeding the myocardium, showing for the first time 3D vasculature patterns inside the myocardium imaged with a sparse array. These preliminary results are the first step towards 3D echocardiography using sparse spiral arrays for the visualization of both the heart chambers and microvessels within the myocardium.

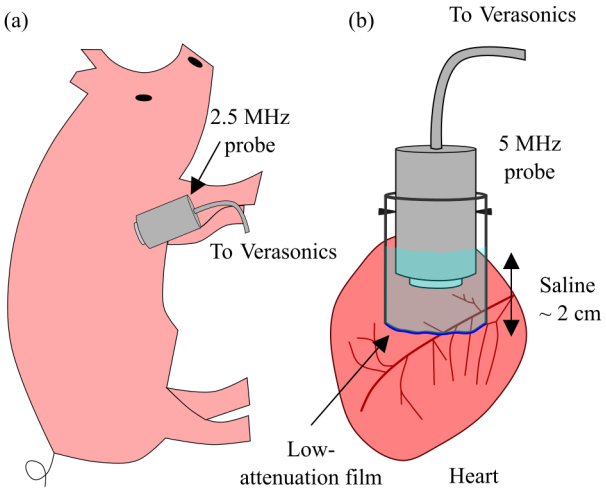

Fig. 1. Schematics of the (a) closed-chest and (b) open-chest experiments. (a) The 2.5 MHz spiral array was directly placed on the pig's skin as it laid on its left side. The probe position and angle was adjusted based on live focused-beam cross-plane images. (b) For the open chest recordings, a saline spacer made up of a plastic cylindrical holder with a piece of low-attenuating ultrasound film was attached to the front of the probe. The film was slack to allow vertical motion of the heart. The probe with spacer was directly placed on top of the exposed heart.

II. Methods

A. Animal Preparations and Imaging Sequences

Two female Yorkshire x Norwegian Landrace pigs (40 and 35 kg) were sedated with intramuscular injections of Zoletil 50 (6 mg/kg), Xylazine (2.25 mg/kg), and Atropine (0.03 mg/kg), anesthetized with intravenous infusion of Pentobarbital (10-15 mg/kg/h), intubated and mechanically ventilated with oxygen enriched room air to maintain arterial blood gas within the physiological range. The animal experiments followed Euro-

This work was part of the research programme "Vernieuwingsimpuls – Vidi 2017" with project number QUANTO-16572, which is (partly) financed by the Dutch Research Council (NWO).

Luxi Wei (e-mail: l.wei@.erasmusmc.nl), Geraldi Wahyulaksana, Maaike te Lintel Hekkert, Daniel Bowen, Robert Beurskens, and Dirk J. Duncker are with the Department of Cardiology, Erasmus MC University Medical Center, the Netherlands. Enrico Boni, Alessandro Ramalli, and Piero Tortoli are with the Department of Information Engineering, University of Florence, Italy. Emile Noothout is with the Department of Imaging Physics, Delft University of Technology, the Netherlands. Antonius F.W. van der Steen, Martin D. Verweij, Nico de Jong, and Hendrik J. Vos are with the Department of Cardiology, Erasmus MC University Medical Center, the Netherlands, and also with the Department of Imaging Physics, Delft University of Technology, the Netherlands.

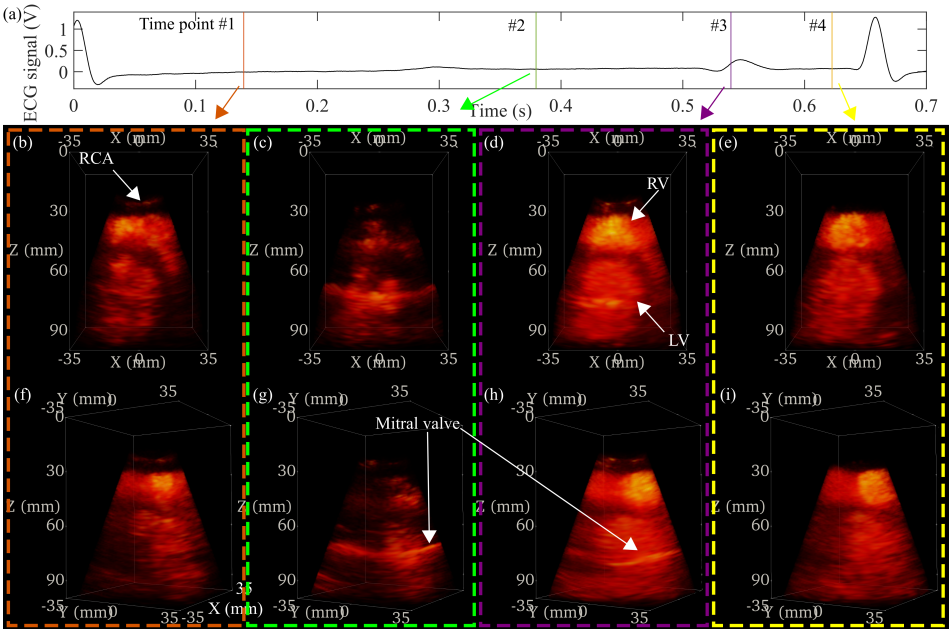

Fig. 2. Closed-chest porcine cardiac volumetric recordings. Using the simultaneously acquired ECG signal (shown in (a)), phases of the cardiac cycle were identified and matched to the volumetric renders (b-i). Time points 1 to 4 on the ECG signal in (a) correspond to the four columns in (b) to (i), where the rows in (b) to (i) show two render orientations. The right (RV) and left ventricles (LV) as well as a segment of the right coronary artery (RCA) could be seen throughout most of the recordings. The mitral valve was visible at time points 2 and 3. The left sides of the images in (f and i) were dark, possibly due to rib shadows.(j) Slices of the end-diastolic heart results. Contours on the three planes (blue, orange, and yellow lines) were drawn on the slices to indicate the volume used for left-ventricular volume calculation.

pean Union and institutional guidelines for the care and use of laboratory animals, with approval (AVD1010020172411; SP2100125). For the closed-chest experiments, a diluted (30x in saline) SonoVue®solution (Bracco Spa, Milan, Italy) was infused through the jugular vein at 2 mL/min flow rate. For the open-chest experiments, a catheter was inserted into the base of the left anterior descending (LAD) artery, and a Definity®(Lantheus Medical Imaging Inc., MA, USA) bolus of 0.1 mL was injected directly into the LAD followed by a 5 mL saline flush before the high-frame-rate acquisitions.

The closed- and open-chest experiments (with two prototype sparse spiral arrays centered at 2.5 and 5 MHz respectively [5]) followed the same imaging sequence [7]. Both probes were driven by a Vantage 256 system (Verasonics Inc., WA, USA). We transmitted 3-cycle pulses without any contrast pulsing sequences. Five-angled diverging waves (max 5° steering, 40° or 30° opening angle) were transmitted subsequently at a pulse-repetition-frequency (PRF) of 5 Hz, and reaching a final angle-compounded frame rate of 1 kHz. Received radio-frequency (RF) data were filtered around the fundamental frequency. ECG signal was captured simultaneously throughout all recordings.

Closed-chest experiments were performed with the pig lying on its left side, and placing the 2.5 MHz probe directly on the pig's skin and coupled with ultrasound gel (Fig. 1a). For open-chest experiments, sternotomy was performed to expose the heart. A flexible saline spacer made up of low-attenuating ultrasound probe sleeve (Palmedic b.v., Gelderland, NL) was attached to the front of the 5 MHz probe via a 3D printed casing, creating a distance of 2 to 3 cm (depending on the position of the heart) between the probe and the heart surface (Fig. 1b). The probe and spacer system was placed directly above the LAD such that it was in the field of view, with the spacer coupled to the heart with ultrasound gel.

B. Post-processing: Closed-chest Chamber Dynamics

To visualize the microbubbles inside the right and left ventricles, the recorded RF data was first beamformed with delay and sum (DAS), and then filtered using a moving singular value decomposition (SVD) filter. We used 10 frames as the ensemble length, with 90% overlap, and an automatically determined threshold to remove lower ranks that mostly contained tissue clutter signal [8]. Power Doppler processing (with ensemble length of 5 frames and no overlap) was applied to the filtered images.

To estimate end-diastolic volume, 25 end-diastolic frames (25 ms) of a single cardiac cycle were chosen based on the ECG signal and averaged to obtain a smoother chamber shape. Manual segmentation to remove the right ventricle followed by intensity thresholding was used to create a mask of the left ventricle in 3D. The number of voxels within this 3D masked region multiplied by voxel size was calculated as the end-diastolic left-ventricular volume.

C. Post-processing: Open-chest Coronary Flow

Blood flow within the myocardium was visualized in open-chest recordings. RF or DAS-beamformed in-phase and quadrature (IQ) data were filtered using a moving SVD filter (ensemble length 10 frames, removing the first 8 ranks). The filtered RF signal was used to beamform using the spatial coherence (SC) method [7]. These steps were performed for the entire recording which included 3 cardiac cycles.

In order to obtain a more complete vasculature structure, 3D recordings from three cardiac cycles were synchronized using their ECG signals and averaged. A rigid, translational-only motion correction pipeline based on speckle amplitude correlation was used to correct for any displacement between matching time points of the three cardiac cycles [9]. Translational motion in the axial and lateral directions of the unfiltered, DAS-beamformed maximum-intensity projected (MIP)

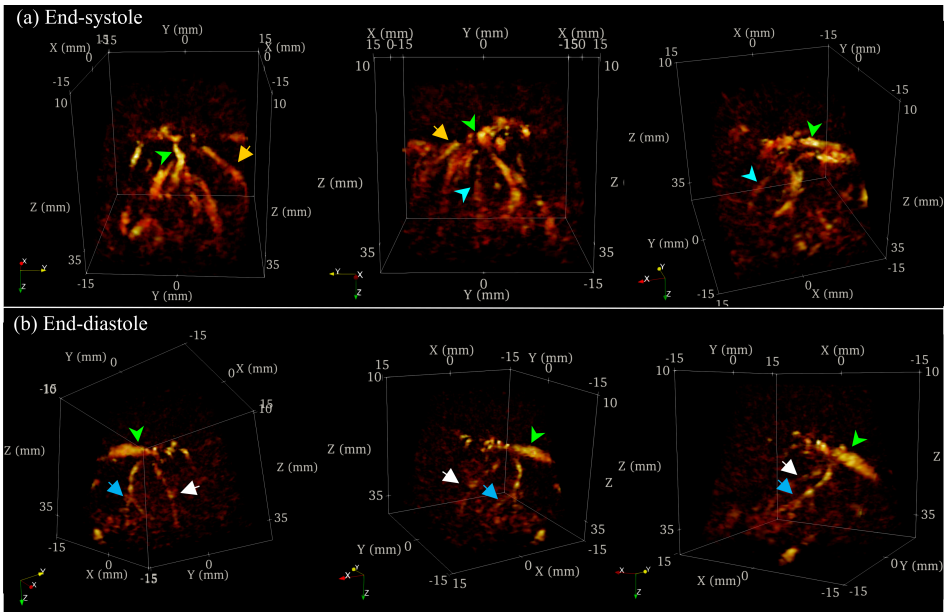

Fig. 3. Renders of the volumetric coronary tree at two time points, corresponding to (a) end-systole and (b) end-diastole. For each time point, three renders of different orientations are displayed for visualization of the 3D structures. The renders are averages of three cardiac cycles, synchronized using the ECG signal. The same color/style arrows point to the same vessel in the three different orientations. The LAD (green arrows) is always in the middle of the field of view due to probe placement. Branches come off of the LAD and into the muscle at multiple locations. Further branching can also be seen (blue arrows). The tree-like structure matches the general physiology of the myocardial vasculature.

images were estimated between frames and used for motion-correction of the SC beamformed volumes. The synchronized and motion-corrected data of the three cardiac cycles were then averaged.

III. Results

Microbubbles moving in the right and left ventricles of the heart could be visualized in the closed-chest recordings. Fig. 2 shows the 3D rendered microbubble signal at four time points (columns) during a cardiac cycle in two orientations (rows), and lined up with their respective time stamps along the ECG trace. The cardiac chambers (right and left ventricles, RV and LV) as well as the septum could be visualized during most of the cardiac cycle. The first row of Fig. 2 was rendered in an orientation that resembled the standard parasternal short axis view using 2D echography, where the circular shape of the septum separates the RV and LV. The second row was less than 90° from the first row. In this view, the RV, the LV and the septum could all be seen. During systole (Time point 1, Fig. 2b,f), the septum was visually thicker than in diastole (time points 3, Fig. 2d,e), which agrees with physiology. Time points 2 and 4 were also in diastole, but the septum was not as visible (Fig. 2c,e,g,i). The chambers became less distinguished at time point 2 (Fig. 2c, g) when the mitral valve opened, giving a high intensity and fast-moving signal. At this time point, the spatial-temporal characteristics of the mitral valve and microbubbles did not allow the SVD filter to fully distinguish the two, leading to more microbubble signal being removed when attempting to remove mitral valve signal. At time point 3, the slower motion of the mitral valve did allow separation from the chamber microbubble signal, leading to the simultaneous visualization of both. The timing of the mitral valve motion relative to the ECG signal agrees with known mitral valve dynamics of a healthy animal.

End-diastolic volume was estimated using the first cardiac cycle of this dataset. Fig. 2j shows three orthogonal slices through the averaged end-diastolic volume as well as the segmented region (color lines). The estimated volume was 41 mL, which is similar to values reported in the literature from pigs of similar weights [10]. Our value is likely an under-estimation of the end-diastolic left ventricular volume because of the incomplete visualization of the chamber due to rib shadowing (Fig. 2f, i).

Fig. 3 shows renders of the vasculature structure inside the myocardium at two time points, end-systole and end-diastole. The LAD can be seen on top (green arrowheads), with smaller arterioles branching off of it. Further branches can also be seen (blue arrows). During end-systole, most vessels could be seen, likely due to low axial and lateral motion. Because of the large non-rigid motion throughout the recording and its changing effects on filter efficacy, quantification on the flow amount would be difficult and likely inaccurate. Nevertheless, branching vascular patterns similar to what was reported in literature could be observed and visualized in 3D *in vivo*.

IV. Discussion

In this paper, we have shown various cardiac volumetric results using two sparse spiral arrays. For the closed-chest experiments, the 2.5 MHz probe was chosen because of its superior penetration depth. With this probe and post-processing filters, we could visualize the microbubbles in the chambers throughout most of the cardiac cycle (Fig. 2). The only exceptions were during peak systole (not shown) and during mitral valve opening (Fig. 2c, g), when the filter failed because of high myocardial motion and the high intensity signals from the mitral valve respectively. In theory, end-diastolic left ventricular volume could also be estimated without any assumptions in the shape of the left ventricle (Fig. 2j). Even though volumetric recordings can give true estimates of left

ventricular volume, several practical issues still remain. Due to the limited maximum opening angle of our prototype probes, the entire heart could not be captured at once. As a result, it was difficult to tell whether the entire left ventricle was in the field of view. Because of the larger footprint of the probe (3 x 3 cm) compared to conventional 2D or even recent 3D probes, there was likely a rib shadow artifact on part of the image. This possibly has led to under-estimation of the end-diastolic volume. Increasing the opening angle by reducing element size and minimizing the footprint of the transducer, rib shadow artifacts can be reduced and may lead to better visualization of the entire left ventricle. Dedicated contrast enhancement pulsing schemes, preferably in combination with probes that have a sufficiently large frequency band to allow second-harmonic imaging, might further improve the contrast to background throughout the entire cardiac cycle.

More vasculature was observed during cardiac phases with lower motion (Fig. 3), but the vasculature that we saw was still incomplete. When there was low cardiac motion, the acquisition frame rate was high enough to enable the SVD filter to distinguish slow-flowing microbubbles from slower-moving tissue, leading to sufficient removal of tissue signal. But microbubbles that were flowing at even slower speeds, such as those in capillaries, still could not be separated from tissue signal. To increase sensitivity to slower-moving microbubbles, longer ensemble lengths are required. Non-rigid motion correction in the IQ domain may improve our filtering abilities. The work from Cormier *et al.* [11] describes a Lagrangian beamformer that performs this correction in 2D. The application of this beamformer in 3D would greatly enhance the filtering abilities of the SVD filter.

V. Conclusion

In this paper, we have demonstrated volumetric cardiac imaging of microbubbles in the right and left ventricles and in the myocardial vasculature. Further hardware and post-processing improvements can enable more accurate assessment of true left ventricular volumes and myocardial blood flow dynamics. Nevertheless, these preliminary results confirm the possibility of performing volumetric high frame rate echocardiography using sparse spiral arrays.

Acknowledgment

The authors would like to thank Mihai Strachinaru (EMC) for preliminary imaging experiments, Joaquim Bobi I Gibert (EMC) and Annemarie Verzijl (EMC) for their support during the animal experiments, and Jason Voorneveld (EMC) for the helpful discussions and code sharing.

References

[1] A. G. Japp, A. Gulati, S. A. Cook, M. R. Cowie, and S. K. Prasad, "The diagnosis and evaluation of dilated cardiomyopathy," *J Am Coll Cardiol.*, vol. 67, no. 25, pp. 2996–3010, 2016.

[2] N. S. Anavekar and J. K. Oh, "Doppler echocardiography: A contemporary review," *J Cardiol.*, vol. 54, no. 3, pp. 347–358, 2009.

[3] M. Dewey, M. Siebes, M. Kachelrieß, *et al.*, "Clinical quantitative cardiac imaging for the assessment of myocardial ischaemia," *Nat Rev Cardiol.*, vol. 17, no. 7, pp. 427–450, Feb. 2020.

[4] J. L. Dorosz, D. C. Lezotte, D. A. Weitzenkamp, L. A. Allen, and E. E. Salcedo, "Performance of 3-dimensional echocardiography in measuring left ventricular volumes and ejection fraction: A systematic review and meta-analysis," *J Am Coll Cardiol.*, vol. 59, no. 20, pp. 1799–1808, 2012.

[5] L. Wei, E. Boni, A. Ramalli, *et al.*, "Sparse 2-dimensional PZT-on-PCB arrays with density tapering," *IEEE Trans. Ultrason. Ferroelectr. Freq. Control*, Oct. 2022.

[6] A. Ramalli, E. Boni, E. Roux, H. Liebgott, and P. Tortoli, "Design, implementation, and medical applications of 2-D ultrasound sparse arrays," *IEEE Trans. Ultrason. Ferroelectr. Freq. Control*, pp. 1–1, Mar. 2022.

[7] L. Wei, G. Wahyulaksana, B. Meijlink, *et al.*, "High frame rate volumetric imaging of microbubbles using a sparse array and spatial coherence beamforming," *IEEE Trans. Ultrason. Ferroelectr. Freq. Control*, vol. 68, no. 10, pp. 3069–3081, Oct. 2021.

[8] J. Baranger, B. Arnal, F. Perren, O. Baud, M. Tanter, and C. Demene, "Adaptive spatiotemporal SVD clutter filtering for ultrafast Doppler imaging using similarity of spatial singular vectors," *IEEE Trans. Med. Imaging*, vol. 37, no. 7, pp. 1574–1586, Jul. 2018.

[9] E. A. Pnevmatikakis and A. Giovannucci, "NoRMCorre: An online algorithm for piecewise rigid motion correction of calcium imaging data," *J. Neurosci. Methods*, vol. 291, pp. 83–94, Nov. 2017.

[10] C. J. Gallup, S. E. Cabreriza, J. P. Hart, R. Walsh, A. Weinberg, and H. M. Spotnitz, "Left ventricular end-diastolic volume from ejection fraction and stroke volume in pigs during ivc occlusion," *J Surg Res.*, vol. 106, pp. 76–81, 1 Jul. 2002.

[11] P. Cormier, J. Poree, C. Bourquin, and J. Provost, "Dynamic myocardial ultrasound localization angiography," *IEEE Trans. Med. Imaging*, vol. 40, pp. 3379–3388, 12 Dec. 2021.